MULTICHANNEL ±1.16 KV ARBITRARY WAVEFORM GENERATOR FOR DRIVING MULTISTAGE FERROELECTRIC LASER-BEAM-DEFLECTOR

by

Fikri Muhammad

A thesis submitted to the Faculty of the University of Delaware in partial fulfillment of the requirements for the degree of Master of Science in Electrical and Computer Engineering

Winter 2006

Report Documentation Page

Form Approved
OMB No. 0704-0188

1. REPORT DATE	2. REPORT TYPE	3. DATES COVERED
2006		**00-00-2006 to 00-00-2006**

4. TITLE AND SUBTITLE	5a. CONTRACT NUMBER
MultiChannel +-1.16 KV Arbitrary Waveform Generator for Driving Multistage Ferroelectric Laser-Beam-Deflector	5b. GRANT NUMBER
	5c. PROGRAM ELEMENT NUMBER
6. AUTHOR(S)	5d. PROJECT NUMBER
	5e. TASK NUMBER
	5f. WORK UNIT NUMBER
7. PERFORMING ORGANIZATION NAME(S) AND ADDRESS(ES) **University of Delaware,Department of Electrical and Computer Engineering ,Newark,DE,19716**	8. PERFORMING ORGANIZATION REPORT NUMBER
9. SPONSORING/MONITORING AGENCY NAME(S) AND ADDRESS(ES)	10. SPONSOR/MONITOR'S ACRONYM(S)
	11. SPONSOR/MONITOR'S REPORT NUMBER(S)

12. DISTRIBUTION/AVAILABILITY STATEMENT
Approved for public release; distribution unlimited

13. SUPPLEMENTARY NOTES

14. ABSTRACT
see report

15. SUBJECT TERMS

16. SECURITY CLASSIFICATION OF:			17. LIMITATION OF ABSTRACT	18. NUMBER OF PAGES	19a. NAME OF RESPONSIBLE PERSON
a. REPORT **unclassified**	b. ABSTRACT **unclassified**	c. THIS PAGE **unclassified**	**Same as Report (SAR)**	**69**	

MULTICHANNEL ±1.16 KV ARBITRARY WAVEFORM GENERATOR FOR DRIVING MULTISTAGE FERROELECTRIC LASER-BEAM-DEFLECTOR

by

Fikri Muhammad

Approved: _____
Fouad Kiamilev, Ph.D.
Professor in charge of thesis on behalf of the Advisory Committee

Approved: _____
Gonzalo R. Arce, Ph.D.
Chair of the Department of Electrical and Computer Engineering

Approved: _____
Eric W. Kaler, Ph.D.
Dean of the College of Engineering

Approved: _____
Conrado M. Gempesaw II, Ph.D.
Vice Provost for Academic and International Programs

ACKNOWLEDGMENTS

I want to thank Professor Fouad Kiamilev, Ph.D., for his continuous advice, guidance, and academic support during my study at the University of Delaware. I must also thank my friends and colleagues, who have supported and helped me throughout my graduate education. I thank my parents and my brothers for their endless love and support.

The work in this thesis was supported by the Defense Advanced Research Projects Agency (DARPA) Steered Agile Beam (STAB) program through contract No. N66001-00-C-8087 from Space and Naval Warfare (SPAWAR) Systems Center San Diego. I also gratefully acknowledge Xilinx, Inc. for their donation of VHDL synthesis and FPGA programming software.

TABLE OF CONTENTS

LIST OF FIGURES

LIST OF TABLES

ABSTRACT

Ferroelectric laser-beam-deflector has become one of the favorite devices for laser beam steering because of its ability to steer a laser beam without moving parts, its relatively high frequency of operation, and its large deflection angle. Furthermore, using multiple stages of ferroelectric beam deflector, the maximum deflection angle can be increased dramatically. However, these attractive features come with the cost of high drive-voltage requirement. Additionally, a multistage beam deflector requires a multichannel driver with output channel synchronization capability. This thesis presents the first arbitrary waveform generator designed to fulfill all of these drive requirements. The main feature of this waveform generator is its five synchronizable output channels, each capable of producing an arbitrary signal with a voltage of up to ±1.16 kV, a maximum drive current of 10 mA, at a frequency of up to 10 kHz, with 16-bit resolution. The design is implemented using a Field-Programmable Gate Array (FPGA), making it highly reconfigurable and flexible to adapt to different types of application. This waveform generator has been successfully demonstrated to drive a two-stage ferroelectric beam deflector, producing a deflection angle of ±12.7°—a total of 25.4°. Deflection angle this large is unprecedented for electro-optic scanning [1]. A much larger deflection angle is still possible by utilizing all of the five output channels to drive a five-stage ferroelectric beam deflector.

Chapter 1

INTRODUCTION

This thesis presents the design of a multichannel arbitrary waveform generator that is suitable for driving multistage ferroelectric laser-beam-deflectors. This work has been published previously in Photonics Technology Letters, a refereed journal circulated by the Institute of Electrical and Electronics Engineers (IEEE) [2]. It has also been presented in the 14^{th} IEEE/LEOS Annual Meeting Conference, a major conference on lasers and electro-optics organized by the IEEE Lasers and Electro-Optics Society (LEOS) [3]. In addition to that, the Department of Electrical and Computer Engineering at the University of Delaware requires all of its graduate students to present their researches in one of the graduate research seminars held by the department. The work in this thesis has been presented twice in the department's Digital Systems Seminar series.

1.1 Overview

The work discussed here is a part of a larger-scaled research conducted in collaboration with several other organizations to develop the most efficient method for steering a laser beam. The techniques developed in this research can be used in a broad range of applications, such as optical communications, optical signal processing, optical data storage, object detection and ranging, visual effects and display, document scanning, and laser printing. Although the ferroelectric device driver described in this thesis was originally developed for use in the area of avionic

countermeasures, the flexibility of its design allows it to be used in other types of applications as well.

1.1.1 Integrated Beam Steering Device

There are several methods that can be used to steer a laser beam. The most straightforward method is by using motorized mirrors to reflect the laser beam toward the desired direction. These motorized mirror modulators have some major drawbacks. They take a lot of space and draw a large amount of energy. They are also heavy, and relatively slow in operation. In order to gain significant improvements on these aspects of performance, it is essential to use a much smaller device. There are some micro-sized devices that can be used, including Spatial Light Modulators (SLMs), liquid crystals, ferroelectric beam deflectors, micro-mirrors controlled using Micro-Electro-Mechanical System (MEMS), acousto-optic modulators, and photonic crystals. In addition to being small, most of these devices have no moving parts. The elimination of moving parts can help increase the reliability of the device, and reduce both the production and the maintenance costs.

Unfortunately, no single beam steering device is perfect. Each device has its own strengths and weaknesses. Some devices, however, are remarkable in their strengths while also supporting integration with other devices. By combining devices that complement one another, it is possible to devise a solution to serve even the most demanding applications. Among the different beam steering methods available, ferroelectric beam deflectors [1], SLMs [4]–[5], and MEMS-controlled micro-mirrors are the most promising candidates for heterogeneous integration.

SLMs have an excellent beam steering performance. They can operate very fast, yet still retain high resolution. The deflection of the laser beam is two-dimensional, with random access capability. However, they can only cover a narrow spectral bandwidth.

On the contrary, MEMS-controlled micro-mirrors have a broadband spectrum, similar to motorized mirror modulators. The mirror movement is quite flexible as well. Unfortunately, their operating speed is not as high as that of the other devices.

A large deflection angle can be provided by the ferroelectric beam deflectors, albeit only one-dimensional. These devices also have the capability to handle high-powered laser. On the other hand, they need to be driven using high voltage signals. This may not be desirable for some applications.

1.1.2 Device Driver Development

As part of the project to build a heterogeneously integrated beam steering device, the work in this thesis is a stage in the development of the driver for the ferroelectric device. The need to build this driver arose because there was no equipment capable of driving multistage ferroelectric beam deflectors. This type of deflector requires multichannel high-voltage outputs with channel synchronization capability. Previously, multistage ferroelectric beam deflectors were driven by using a waveform generator with unsynchronized outputs. These output channels have to be controlled manually. This manual operation can only be employed for laboratory testing purposes. For real world operations, the channel synchronization has to be done automatically.

The ferroelectric beam deflector used in the project discussed here is made from lithium tantalate ($LiTaO_3$). It is developed by other researchers at the Pennsylvania State University (PSU) [6]. Due to the collaborative nature of the research, other organizations were involved in specifying the requirements of the ferroelectric device driver discussed in this thesis. In addition to PSU, there were also BAE SYSTEMS, and the Los Alamos National Laboratory (LANL).

Those organizations were also involved during the system testing phase. A system test was conducted to examine the capability of the driver to control a

ferroelectric beam deflector. For this test, a demonstration system composed of the beam deflector and the ferroelectric device driver was set up at the LANL facility. PSU provided all the optical instruments necessary for the demonstration, and BAE SYSTEMS acted as the event organizer.

1.2 Thesis Outline

This thesis is divided into five chapters. The first chapter serves as an introduction to the thesis. It provides an overview of the thesis and the background of the research work. The structure of the thesis with the summary of each chapter can also be found in this chapter.

It is not easy to find a simple introductory literature on ferroelectricity. Most of the published books are written for someone with material science background. For this reason, a short and easy-to-understand, yet relatively complete introduction to ferroelectricity is provided in the second chapter. The chapter begins with an explanation of the unique polarization properties that differentiates ferroelectric materials from materials of other type. After that, the chapter discusses the different mechanisms of polarization in materials. The effects of polarization in crystals with different structures are described afterward. In the final part of the chapter, some applications of ferroelectricity are mentioned. A number of specific terms in ferroelectricity are introduced along the way.

In the third chapter, the application of ferroelectric materials for beam steering is discussed. An emphasis is given on the $LiTaO_3$ and lithium niobate ($LiNbO_3$) crystals and their use for beam deflectors. Moreover, the beam deflector device concept and its fabrication are explained. Then, a discussion on the driver requirements for the beam deflector device concludes this chapter.

Chapter four explains the design of a multichannel waveform generator for driving multistage ferroelectric beam deflector. This chapter contains the main research work done by the author. It starts with the discussion on the requirements,

the specifications, and the features of the design. The architecture of the design is presented next. Further, each subsystem within the driver is described in detail. This chapter ends with a discussion on the system testing of the driver.

The last chapter talks about the possible directions that can be explored in the future. The possibility of integrated circuit implementation is investigated. Several high-voltage process technologies are evaluated to examine the possibility of implementing the driver on an Integrated Circuit (IC) chip.

Chapter 2

FERROELECTRICITY IN MATERIALS

It has been more than 80 years since ferroelectricity was first discovered. Within this period, numerous efforts have been carried out to understand this phenomenon. Researches have also been conducted to explore the potential applications of ferroelectricity. As a result, today the utilization of ferroelectric materials (*ferroelectrics*), mainly for optoelectronic and imaging devices, has been successfully commercialized.

2.1 Ferroelectric Effect

Ferroelectricity was first recognized in Seignette salt, also known as Rochelle salt ($NaKC_4H_4O_6{\cdot}4H_2O$). For this reason, at its early age, this phenomenon was known as Seignette-electricity. Only later, when more crystals with the same properties were discovered, the term "ferroelectricity" became more popular.

In 1920, Joseph Valasek reported that the dielectric properties of this crystal were analogous to the ferromagnetic properties of iron [7], [8]. He noticed the similarity by observing the polarization of the salt produced by an electric field applied on it. This polarization is measured as electric moment per unit volume.

The observation of ferroelectric effect can be done reliably using the Sawyer-Tower circuit [9] shown in Figure 2.1. An AC voltage source is used to generate a varying electric field. The output of this voltage source is applied to a ferroelectric crystal sample with internal capacitance and resistance, C_X and R_X, respectively.

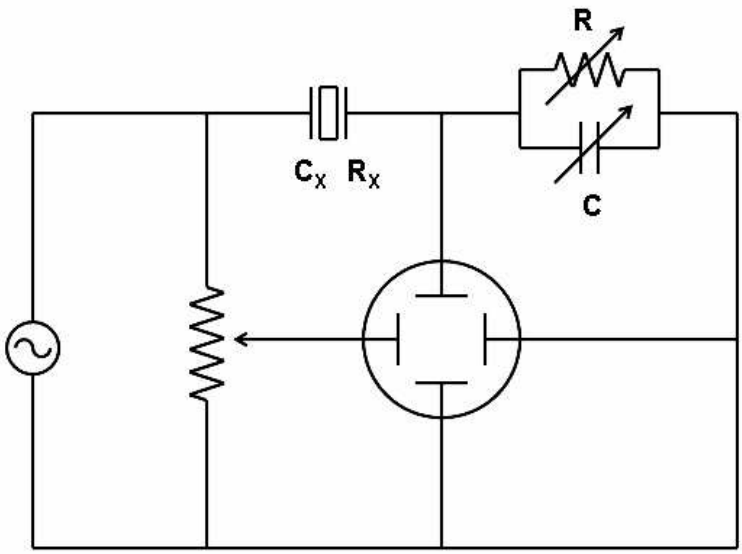

Figure 2.1: Sawyer-Tower circuit for observing polarization

In order to find the electric field experienced by the sample, a trimmer potentiometer (trimpot) is connected parallel to the source. The voltage across this trimpot is fed to an oscilloscope to be displayed in the horizontal axis. Variable resistor (varistor) R and variable capacitor C are used to compensate for any phase shift due to conductivity or dielectric loss in the sample [10]. The voltage across capacitor C is proportional to the polarization of the crystal sample. This voltage is fed to the oscilloscope, and displayed in the vertical axis.

The curve resulted from this experiment exhibits a hysteresis loop that is similar to the one obtained in the magnetization of iron caused by an applied magnetic field. Figure 2.2 shows a typical ferroelectric hysteresis curve. More details on the mechanism behind this phenomenon will be discussed in Section 2.4.

Another similarity between ferroelectricity and ferromagnetism is the presence of a *Curie point*. The ferroelectricity phenomenon can only occur within the

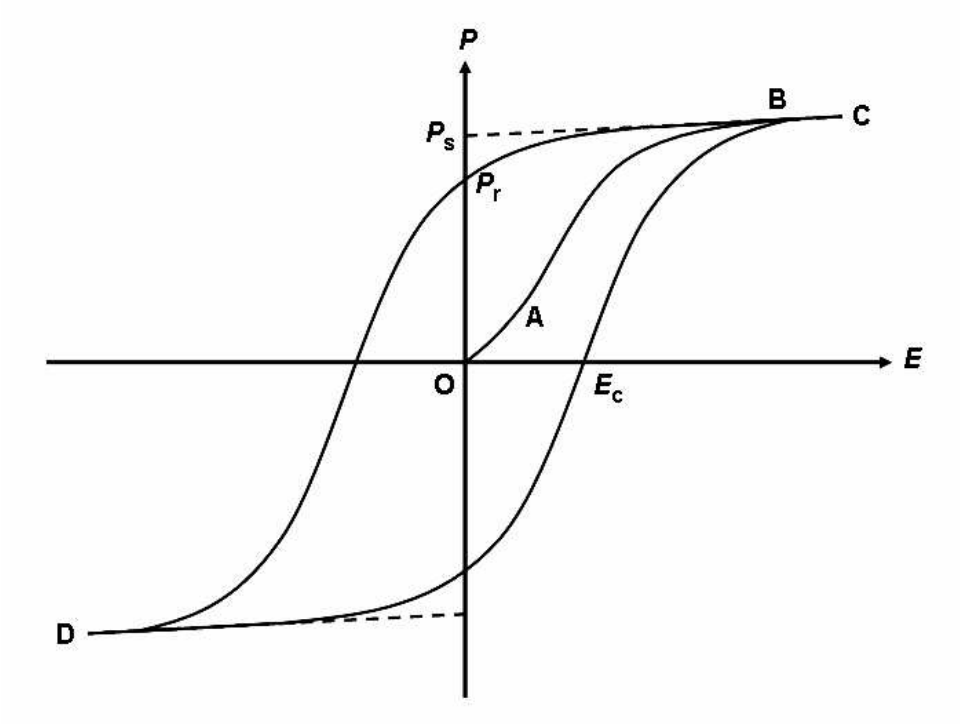

Figure 2.2: Typical hysteresis loop for ferroelectrics

temperature range below this point. At a Curie point, the molecular structure of a ferroelectric material slightly changes. Above this point, the material loses its ferroelectric properties and its dielectric constant varies with temperature following the Curie-Weiss law:

$$\epsilon = \frac{C}{T - \theta}$$

where C and θ are constants, specific to the material.

Because of those similarities to ferromagnetism, the term "*ferroelectricity*" was coined. This term, however, can be confusing, because the phenomenon is not directly related to *ferrum* (iron), but merely analogous to ferromagnetism.

Polarization is one of the main topics in the study of dielectric materials (*dielectrics*). In order to get more details on the polarization of materials, an overview of dielectric materials and their polarization properties needs to be discussed.

2.2 Polarization in Dielectric Materials

The study of dielectric materials emerged at the time of early electrostatic experiments, when there was a need for insulating materials (*insulators*). These materials do not conduct electrostatic charges, and they can increase the charge-storage capacity of a condenser. Certainly, each material has its own *dielectric strength*. It is defined as the minimum strength of an applied electric field, under which an uncontrollable current would flow through the material.

A dielectric material increases the charge-storage capacity of a condenser by neutralizing some of the charges at the electrode surfaces through polarization. This polarization phenomenon was first recognized by Michael Faraday. It can be visualized as the formations of *dipole* chains induced by an applied electric field [12] as illustrated in Figure 2.3.

The figure shows a dielectric material placed between two metal electrodes. Positive charges are being conducted to the electrode at the top. The bottom

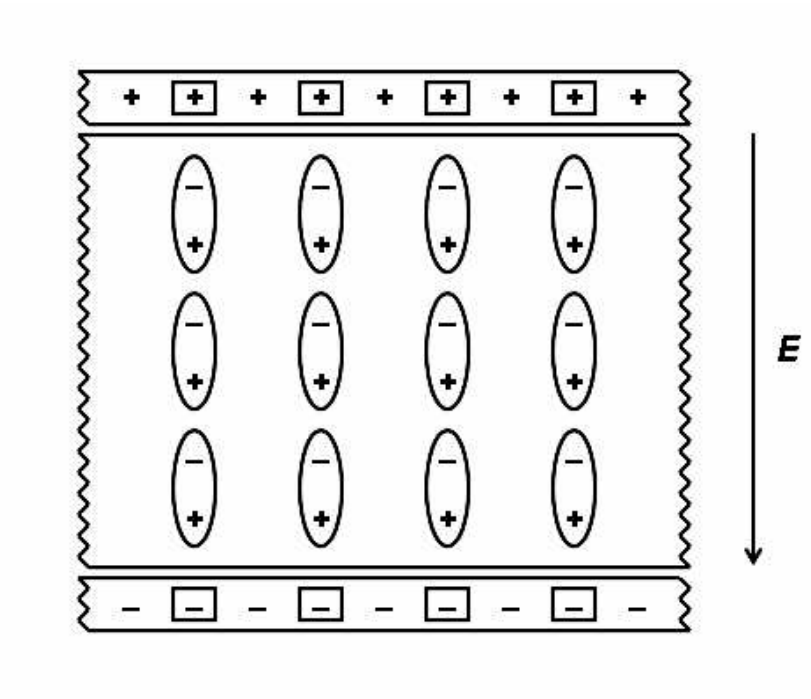

Figure 2.3: Polarization in dielectric materials

electrode is filled with negative charges. Electric field is formed with the direction from top to bottom. Dipole chains then formed inside the dielectric material. Some of the charges on the metal surfaces are bound by the free ends of these dipole chains.

Polarization can be defined as a limited displacement of charge by an electric field. It is usually produced as the result of a combination of different atomic and molecular processes. According to the molecular structures of dielectrics, mechanisms of polarization can be classified into three different types: *electronic*, *molecular*, and *space-charge polarization* [14].

2.2.1 Electronic Polarization

An atom is made up from a positively charged nucleus surrounded by clouds of negatively charged electrons. Under the influence of an electric field, the electron clouds and the nucleus are shifted in opposite directions. The displacement creates an induced dipole moment. This type of polarization occurs extremely quickly, usually at visible light or higher frequencies. Sometimes electronic polarization is also called *optical polarization*. Figure 2.4 illustrates the electronic polarization of an atom.

2.2.2 Molecular Polarization

When two atoms of different types bond together, their electrons are not distributed symmetrically. They are attracted toward the atom with higher electronegativity. This close proximity to electrons causes this atom to become more negative than the other. A dipole moment is then created. This dipole moment resides permanently inside the molecule.

In a molecule with three or more atoms, the dipole moments from each of the atomic bonds combine into a resultant dipole moment. There are some cases, however, where the structure of the molecule is symmetrical, causing the constituent

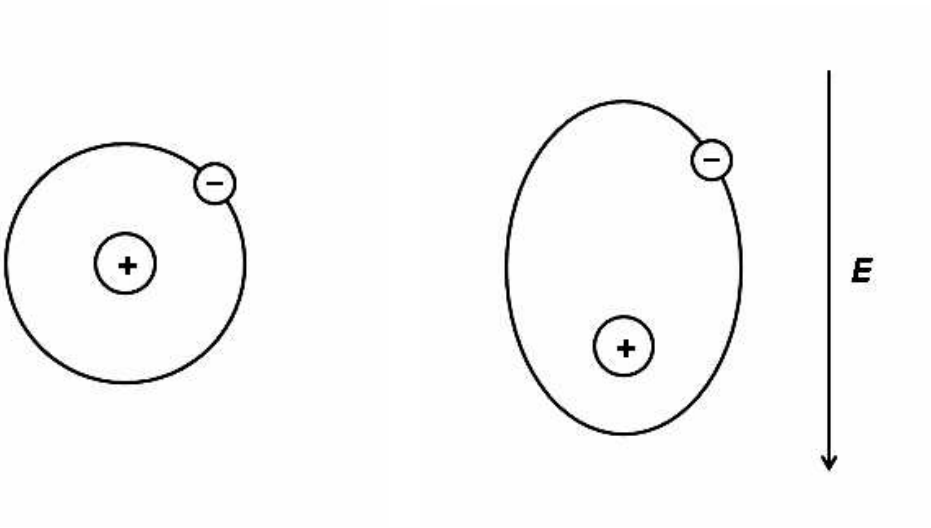

(a) no electric field (b) electric field present

Figure 2.4: Electronic polarization of an atom induced by the presence of an electric field

dipole moments to cancel each other. As a result, molecules of this type do not have a net dipole moment.

Molecules with permanent dipole moment are frequently referred as *polar* molecules. When an electric field is applied on a polar molecule, *atomic* and *orientational polarization* may occur.

2.2.2.1 Atomic Polarization

Atomic polarization occurs when the atoms inside a polar molecule are displaced with respect to each other. The distance between them is changed. This, in turn, changes the dipole moment. An atomic polarization is illustrated in Figure 2.5.

2.2.2.2 Orientational Polarization

Upon the application of an electric field, orientational polarization causes the permanent dipole of a molecule to reorient itself according to the field direction.

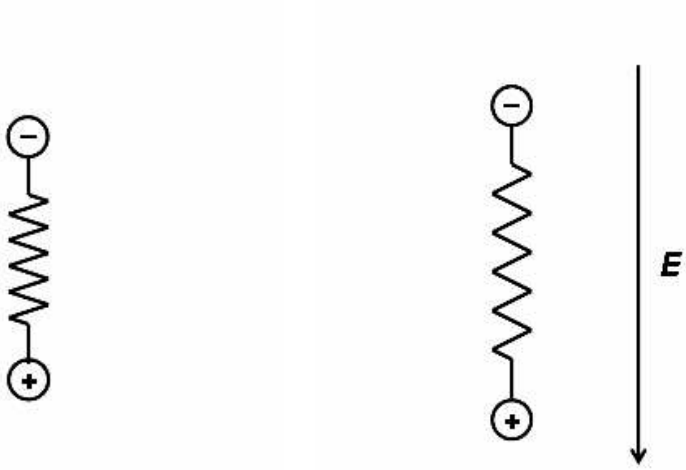

(a) no electric field (b) electric field present

Figure 2.5: Structural change caused by induced atomic polarization

This reorientation causes a change of dipole moment. Figure 2.6 illustrates the orientational polarization in a dielectric material.

2.2.3 Space-Charge Polarization

Charge carriers are moved when subjected to electric field. They can be trapped by defects (lattice vacancies, impurity centers, dislocations, etc.) or interfaces. They may also not be freely discharged or replaced at electrodes. This lump of carriers creates space charges and macroscopic field distortion, inducing charges on an electrode. Sometimes space-charge polarization is also called *interfacial polarization*. This type of polarization is illustrated in Figure 2.7.

At certain temperature, some dielectrics can be polarized without the application of an electric field. They are said to be *spontaneously polarized*. This phenomenon occurs only in some special classes of crystals. The dielectric properties of crystals are discussed more thoroughly in the following section.

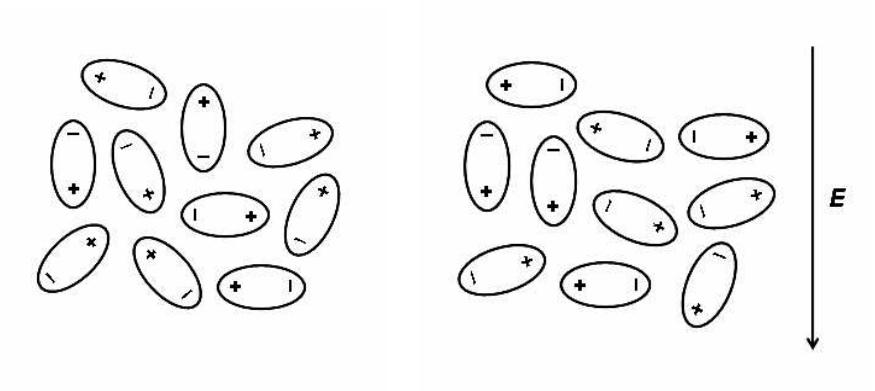

(a) no electric field (b) electric field present

Figure 2.6: Orientational polarization of molecules induced by an electric field

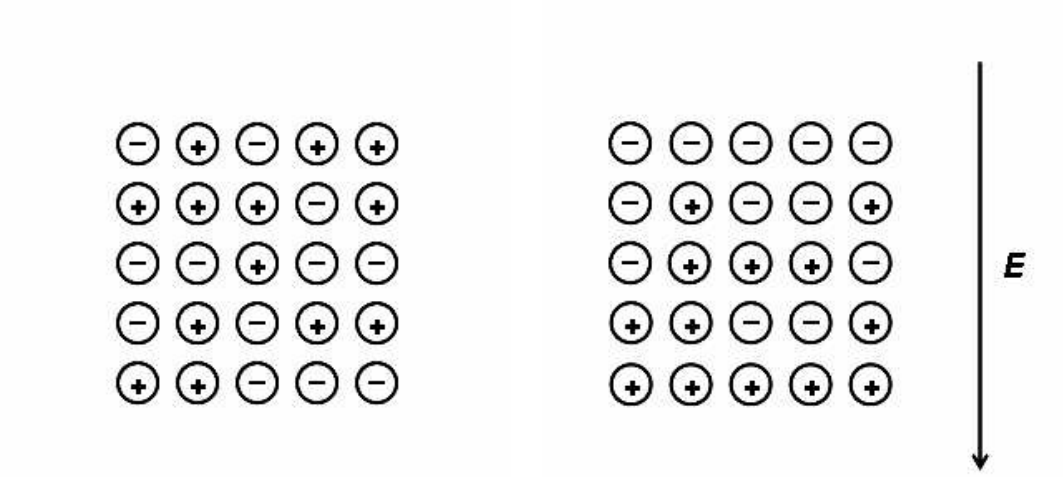

(a) no electric field (b) electric field present

Figure 2.7: Space-charge polarization in a material induced by the presence of an electric field

2.3 Dielectric Properties of Crystals

A crystal can be defined as a regular polyhedral form, bounded by smooth faces, which is assumed by a chemical compound, due to the action of its interatomic forces, when passing, under suitable conditions, from the state of a liquid or gas to that of a solid [15]. In simpler words, a crystal is a material in the solid state, bounded by flat planes. Substances in the liquid and gaseous state can be *crystallized* by turning them into solids first.

There is an interesting anomaly, however. Some materials have a special state between solid crystal and liquid. In this state, these materials take the form of its container just like liquid, but their molecules are arranged uniformly like those in solid crystal. Accordingly, these materials are called *liquid crystals*.

2.3.1 Classes of Crystal

According to their geometry, crystals are classified into seven systems: triclinic, monoclinic, orthorhombic, tetragonal, trigonal, hexagonal, and cubic. They can further be sub-divided into 32 *crystal classes*[1] depending on the elements of symmetry that they have [16].

The thirty two classes of crystal are listed in Table 2.1. Some literatures combine trigonal and hexagonal systems into one single system. In this type of classification, there are only six crystal systems instead of seven.

2.3.2 Effects of Polarization in Crystals

The structural difference in crystals causes them to react differently to an application of electric field. This leads to different effects of polarization for different types of crystal.

[1] Some literatures use the term "*point group*" instead of crystal classes.

Table 2.1: Classification of crystals

Crystal System	**Crystal Class Symbol**		**Centrosymmetric**	**Piezoelectric**	**Pyroelectric**
	International	**Schoenflies**			
Triclinic	1	C_1		√	√
	$\overline{1}$	C_i	√		
Tetragonal	4	C_4		√	√
	$\overline{4}$	S_4		√	
	4/m	C_{4h}	√		
	422	D_4		√	
	4mm	C_{4v}		√	√
	$\overline{4}$2m	D_{2d}		√	
	(4/m)mm	D_{4h}	√		
Hexagonal	6	C_6		√	√
	$\overline{6}$	C_{3h}		√	
	6/m	C_{6h}	√		
	622	D_6		√	
	6mm	C_{6v}		√	√
	$\overline{6}$2m	D_{3h}		√	
	(6/m)mm	D_{6h}	√		
Monoclinic	2	C_2		√	√
	m	C_s		√	√
	2/m	C_{2h}	√		
Orthorhombic	222	D_2		√	
	mm2	C_{2v}		√	√
	mmm	D_{2h}	√		
Trigonal	3	C_3		√	√
	$\overline{3}$	S_6	√		
	32	D_3		√	
	3m	C_{3v}		√	√
	$\overline{3}$m	D_{3d}	√		
Cubic	23	T		√	
	m3	T_h	√		
	432	O			
	$\overline{4}$3m	T_d		√	
	m3m	O_h	√		

2.3.2.1 Electrostriction

From the thirty two classes of crystal, eleven are *centrosymmetric*. Crystals belonging to these classes have a center point of symmetry. They do not exhibit polar properties. An application of electric field induces some atomic movements in the molecules which cause a mechanical deformation of the material (compression or expansion). However, due to the symmetry, the movement of an atom at one side of the molecule is compensated by the movement of another atom at the opposite side. Therefore, the process cannot be reversed, i.e., forcing atomic movement by applying pressure to the crystal does not induce electrical polarity. Because of the symmetry, the same mechanical deformation is produced regardless of the direction of the applied field. This phenomenon is known as *electrostriction*. Electrostriction is common to all dielectric solid materials, not limited to crystals.

2.3.2.2 Piezoelectricity

Twenty out of the twenty one classes of crystals that do not have center of symmetry exhibit electrical polarity when subjected to stress. The stress causes a separation of the centers of gravity of the positive and negative charges, which results in polarization. If the stress is reversed, the polarity also reverses. These materials are called *piezoelectric* materials. The remaining one class, the crystal class 432, does not show this property because it has other elements of symmetry that combine to eliminate the possibility to exhibit this property.

2.3.2.3 Pyroelectricity

From the twenty classes that shows piezoelectricity, ten have a unique polar axis. The dipoles are arranged in such a way so that their moments do not cancel each other. They exhibit spontaneous polarization. Usually, this polarization cannot be detected, because the electric charges are conducted away. However, a temperature change can cause thermal expansion or contraction effect, which induces a

voltage across a crystal, opposite in sign for heating and cooling. The polarization voltage can be detected by measuring the flow of charge to and from the surface. This property is called *pyroelectricity* due to the temperature dependence.

2.3.2.4 Ferroelectricity

Those materials above are called ferroelectric if it has two or more orientational states in the absence of an electric field and can be shifted from one orientational state to another by an electric field. This is possible because of the existence of multiple equilibrium positions. Ions or other charged particles can jump from one position to another if provided the energy necessary to overcome the energy barrier.

Usually, in its initial state, a ferroelectric crystal specimen consists of multiple number of regions. In each of these regions, dipoles are arranged uniformly. The orientation of these regions, however, is randomly distributed in the two or more orientational states mentioned previously. As a result, there is no net bulk polarization.

Like in ferromagnetism, these regions are called *domains*. The domain structure of a crystal can be arranged by *poling*. Poling is done by applying a large electric field in the appropriate direction across the crystal. If a single crystal is needed, the electric field should be applied while taking the crystal through the Curie point, from the higher temperature to the lower temperature. Because of the resemblance to the transition in ferromagnetic materials, during the poling process, the crystal is commonly considered to undergo a transition from *paraelectric* phase to ferroelectric phase.

Other than ferroelectricity, there are also known phenomena called *antiferroelectricity* and *ferrielectricity*. As their name imply, these phenomena are analogous to antiferromagnetism and ferrimagnetism. A material is antiferroelectric when the permanent electric dipoles in opposition completely balance out.

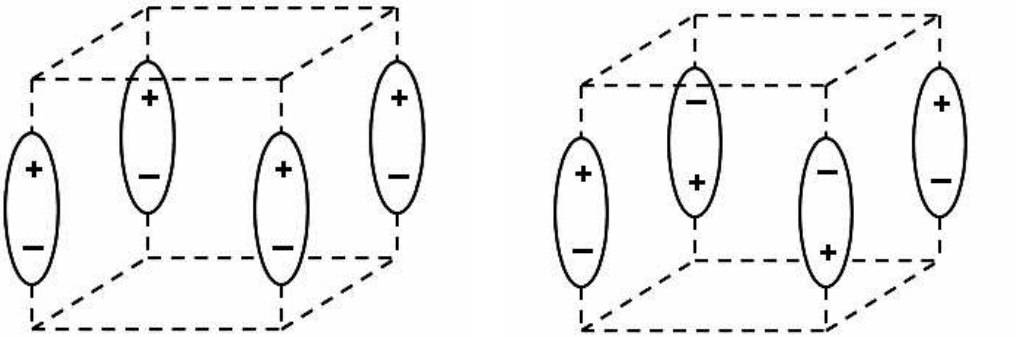

(a) parallel (b) antiparallel

Figure 2.8: Parallel and antiparallel dipole arrays

Figure 2.8(b) shows the dipole arrangement of antiferroelectrics. It can be thought of as a lattice with two sub-lattices, where the sub-lattices are antiparallel to each other.

Sometimes a material still shows ferroelectric properties although it has antiparallel dipole arrangement in it. This material is then called a ferrielectric material. This might happen because the antiparallel dipoles do not cancel each other. It is also possible that the material is ferroelectric in one axis and antiferroelectric in another.

2.4 Hysteresis in Ferroelectric Materials

Let us revisit the ferroelectric hysteresis loop mentioned in Section 2.1 (see Figure 2.2). The detail of the mechanism that causes this phenomenon is explained below.

As the experiment with the Sawyer-Tower circuit progresses, the curve traces as follows. From point O to A, the material behaves like other dielectrics. It shows

a linear relationship between polarization and the applied electric field. The crystal is in *paraelectric* state. In this state, there is only one value of polarization for every value of electric field. The domains inside the material have not yet switched their ferroelectric state because the electric field is not strong enough. As the electric field is increased, the polarization also increases. If the field is reduced again, the polarization value will trace the same curve backward.

When the electric field is further increased, a dielectric non-linearity appears. The crystal starts to switch into a ferroelectric state. In ferroelectric state, polarization P is a double function of electric field E. The domains inside the material begin to reorient themselves according to the direction of the applied electric field.

Each of the domain aligned in the direction of the electric field helps in realigning the other domains, causing an acceleration in the polarization process. The rate of increase gets smaller after all domains are switched into roughly the same direction. Additional process continues with fine realignment.

It finally reached a state of saturation between point B and C. In this state, all domains are in the same direction. Additional polarization increase is caused by electronic and atomic polarizations. If a straight line is drawn passing through point C and B, it intersects the P axis at P_{s}. This point is called the *saturation polarization* value of the material.

When the applied field is decreased, the polarization decreased slowly. The curve intersects the P axis at P_{r}. This point is the *remanent polarization* value of the material. As the field is decreased below zero (reverse direction), the domain switching process begins. At one point, the polarization hits zero, reverses, and then increases in the opposite direction. Finally it reaches the other saturation state at point D. If the field is increased again, the polarization increased slowly. And then, after the field goes above zero, the polarization increase faster. It finally reaches point B, and then C again. The electric field needed to neutralize the polarization

of a ferroelectric from its remanent value is called *coercive field* E_c.

2.5 Applications of Ferroelectricity

There are different types of ferroelectric materials. These materials can be used for a wide range of applications. Various literatures discuss different ferroelectric materials and their applications.

As mentioned previously, ferroelectrics are also dielectrics, piezoelectrics, and pyroelectrics. They have been successfully used for those properties. For example, Rochelle salt was widely used for piezoelectric transducers, such as sonar detectors, microphones, and phonograph pick-ups. Ammonium dihydrogen phosphate ($(NH_4)H_2PO_4$, or more commonly, ADP) is less temperature sensitive and replaced the role of Rochelle salt in sonar applications during World War II. Barium titanate ($BaTiO_3$) was found to have a very large dielectric constant. In ceramic form, it is very good to be used for high-capacitance condensers.

Ferroelectrics have also been proposed for some other applications, but they were not as successful. Their bistable polarization property is suitable for memory elements. However, the performance is not very good. The switching speed is slow, and the memory decays with repeated use. Scientists have been working on these problems, and the first mass product application has been started by Matsushita in December 2003 [20].

The dielectric constant of a ferroelectric material is very much field dependent. This property can be used in parametric amplifier. Unfortunately, amplifiers made from ferroelectric materials are too lossy.

Lately, the most significant use of ferroelectric materials is in optoelectronics, e.g., thermal and infrared detection and imaging devices, optical waveguides, Surface Acoustic Wave (SAW) substrates, optical memories, modulators and deflectors. Ferroelectrics can also be used with other materials for special applications, such

as ferroelectric-electroluminescent, ferroelectric-photoconductor, and ferroelectric-semiconductor.

Chapter 3

MULTISTAGE ELECTRO-OPTICAL BEAM DEFLECTOR DEVICE

One of the most important applications of ferroelectric materials is their use for beam steering. Using the special properties of some ferroelectric materials, the fabrication of beam steering devices without moving parts is possible. This type of device is desirable for various applications, including high-end graphic arts printing, consumer and business laser printing, document scanning, displays, optical data links, optical storage, and spectroscopy for remote sensing.

3.1 Materials for Beam Steering Device

Several ferroelectric materials can be used for beam steering. Some of the more important ones are lithium niobate ($LiNbO_3$), lithium tantalate ($LiTaO_3$), potassium dihydrogen phosphate (KH_2PO_4 or KDP) and deuterated KDP (KD_2PO_4 or DKDP), and also strontium barium niobate ($Sr_{1-x}Ba_xNb_2O_6$ or SBN). Table 3.1 lists some ferroelectric materials that can be used for beam steering applications and their properties.

3.1.1 Comparison

Compared to other ferroelectric materials, SBN has extremely high electro-optic coefficients. However, it is difficult to grow this crystal with uniform optical properties. In addition to that, the crystal tends to *depole* (lose its polarity) in

Table 3.1: Some ferroelectric materials and their properties

Chemical Formula	**Crystal Class**	**Transition Temperature (°C)**	**Spontaneous Polarization ($\mu C/cm^2$)**
$LiNbO_3$	$\bar{3}$m → 3m	1210	71
$LiTaO_3$	$\bar{3}$m → 3m	665	50
$BaTiO_3$	m3m → 4mm → mm2 → 3m	120, 5, −90	26
$NaNO_2$	mmm → mm2	165	8.5
KH_2PO_4	$\bar{4}$2m → mm2	−150	−4.8
$Sr_{0.6}Ba_{0.4}Nb_2O_6$	(4/m)mm → 4mm → m	75, −213	32
$Ba_2NaNb_5O_{15}$	(4/m)mm → 4mm → mm2	560, 300	40
$K_{0.6}Li_{0.4}NbO_3$	(4/m)mm → 4mm	430	40

the presence of a modulating field. Depoling can be prevented by applying a DC bias field. Unfortunately, application of a field also degrades the optical quality of the crystal due to the electrical conductivity of the crystal and the development of space-charge fields.

Crystals of KDP and DKDP can be grown with high optical quality, provided that they are protected in a water-free environment. For this reason, they are more widely used compared to other ferroelectrics, such as $K(TaNb)O_3$ and $Ba_2NaNb_5O_{15}$, even though their electro-optic coefficients are not quite high. For operation, these crystals need a relatively high voltage and good encapsulation.

The significant advantage of using $LiNbO_3$ and $LiTaO_3$ is that large optical-grade crystals of these materials are relatively easy to make, using the Czochralski method. These crystals also exhibit a strong electro-optic effect, making them the favorite materials to be used for electro-optic applications. Their dark resistivities are sufficiently high, but applications involving light at higher energies (wavelength shorter than about 500 nm) are limited by an *optical-damage effect* as the result of the excitation of photocarriers. Although they still need a high modulating field, the required field is relatively low compared to those required by other ferroelectric crystals.

3.1.2 Lithium Niobate and Lithium Tantalate

Two of the most widely used ferroelectric materials are lithium niobate and lithium tantalate. They have similar structure and properties. These two materials are unique compared to other ferroelectrics, that they are considered as a separate family of ferroelectric crystals. Their applications include Surface Acoustic Wave (SAW) devices, high-frequency and high-temperature transducers, infrared detectors, laser modulators, laser frequency multipliers, optical parameter oscillators, optical waveguides, and high-frequency bandwidth filters. In the next section, their application for beam steering will be discussed.

The Curie temperatures of $LiNbO_3$ and $LiTaO_3$ are relatively high (1210°C for $LiNbO_3$ and 620°C for $LiTaO_3$). Both $LiNbO_3$ and $LiTaO_3$ are stable chemically. They are insoluble in water or organic solvents. $LiNbO_3$ crystal is a colorless or light yellow crystal. It has a melting point of 1240±5°C and a density of 4.64 g/cm^3. The color of $LiTaO_3$ crystal is light yellow-green or colorless. Its melting point is 1650°C, and its density is 7.45 g/cm^3. Unlike $LiNbO_3$, its Curie temperature is far from its melting point.

$LiNbO_3$ and $LiTaO_3$ are uniaxial crystals at all temperatures. They only have a single structural phase transition. In ferroelectric phase at room temperatures, $LiNbO_3$ and $LiTaO_3$ crystals belong to the crystal class 3m in the trigonal crystal system. In the *paraelectric* phase above the Curie temperature, they take a different symmetry, and their class changes to the crystal class $\bar{3}$m.

$LiNbO_3$ and $LiTaO_3$ crystals have a relatively high spontaneous polarization (71 μC/cm^2 for $LiNbO_3$ and 50 μC/cm^2 for $LiTaO_3$, at room temperature). The direction of this spontaneous polarization depends on the location of lithium and tantalum/niobium ion with respect to the oxygen layers. The direction of the ion displacements are perpendicular to these oxygen layers, thus in the same axis as the spontaneous polarization itself. Since the ion displacements only occur in one

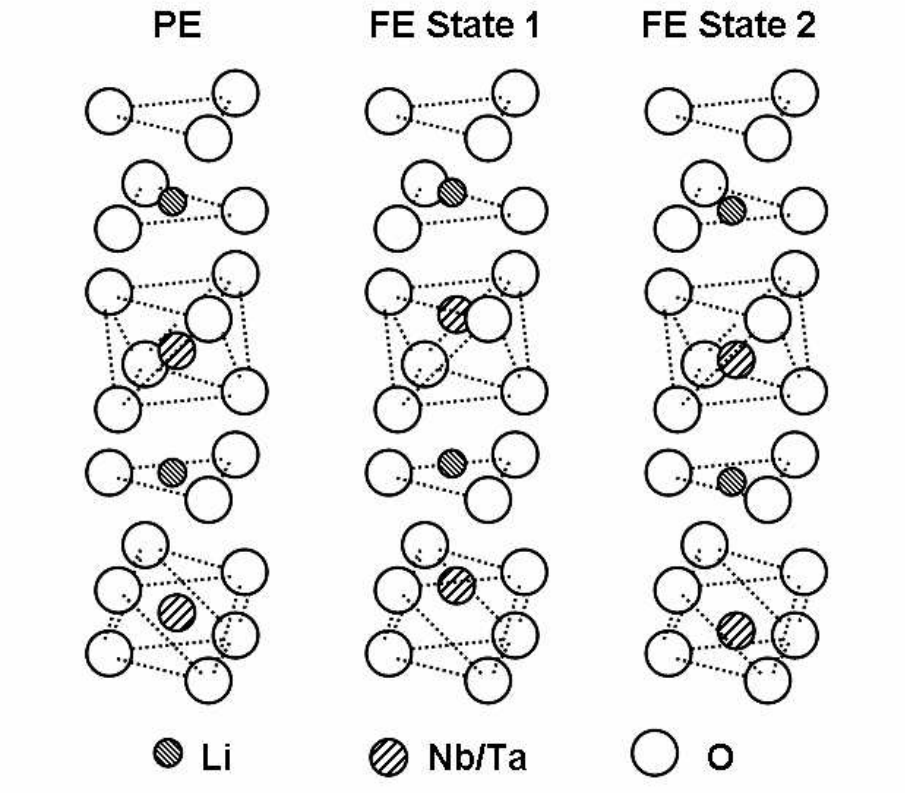

Figure 3.1: Phases of lithium niobate/tantalate

axis, in a crystal there are only two directions of spontaneous polarization, each antiparallel to the other. An illustration of ion displacement in $LiNbO_3$ and $LiTaO_3$ can be seen in Figure 3.1.

Compared to $LiTaO_3$, the domain-wall motion of $LiNbO_3$ during the poling process is relatively unsteady. This unsteady motion causes some difficulties in the implementation of optimized horn-shaped deflector geometries, which will be described in the next section. For this reason, $LiTaO_3$ is preferable for beam deflector devices.

Figure 3.2 shows the hysteresis loop of $LiTaO_3$ [21], which is shaped like a rectangular. Within each polarization state, the crystal maintains a relatively

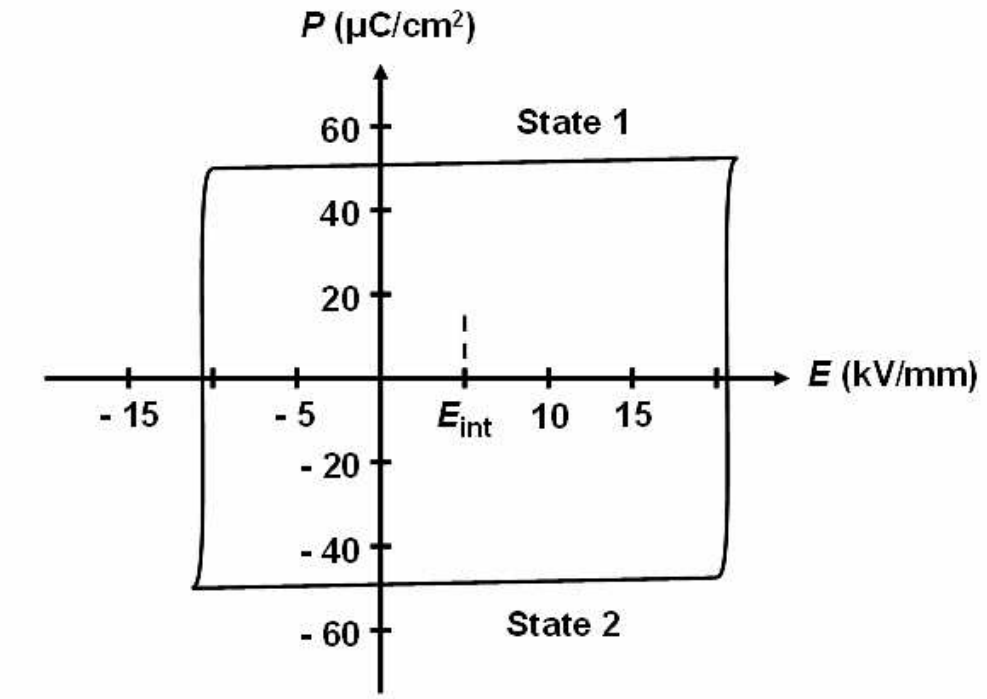

Figure 3.2: The hysteresis loop of lithium tantalate

constant polarization value.

Crystals of $LiTaO_3$ and $LiNbO_3$ are grown using the Czochralski method. In this method, a crystal is grown from a high temperature melt in a crucible. First, a seed crystal is slightly dipped into the surface of the melt. This seed crystal is then rotated and pulled very slowly, allowing the melt to solidify around it. The crystal orientation of the pulled crystal ingot will be the same as that of the seed crystal.

3.2 Device Concept

The refraction index of a poled $LiTaO_3$ crystal can be changed by applying an electric field on it. This is called the *electro-optic effect*. The change of the index of refraction is caused by the distortion in the crystal lattice produced by the

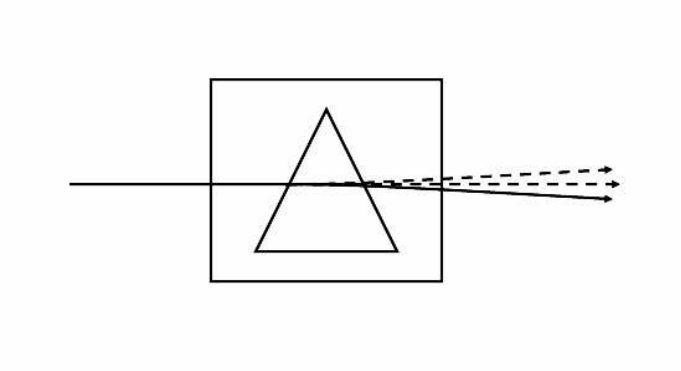

Figure 3.3: A simple beam deflector

applied field [22]. When an electric field is applied in the same direction as that of the spontaneous polarization, the index of refraction decreases. The index will increase if the direction of the electric field is reversed. The relationship can be expressed as:

$$\Delta n_3 = -\frac{1}{2} n_3^3 r_{33} E_3$$

with the subscript 3 denotes the uniaxial direction.

If the ferroelectric domains are arranged in the shape of a prism, a beam that passes through can be steered by controlling the deflection angle of the beam using an electric field. The domains outside of the prism area are poled so that they are antiparallel to the domains inside the prism area. Because there are two oppositely polarized areas involved, the change of the index of refraction seen at the interface between these areas is equal to $2 \times \Delta n_3$. When no electric field is applied, no beam deflection occurs. Application of electric field deflects the beam either to the left or to the right depending on the direction of the electric field. The schematic of a simple deflector device can be seen in Figure 3.3. The continuous line shows the beam path when the applied electric field is at the maximum. The straight dashed line is for no applied field, and the other dashed line is for maximum negative field.

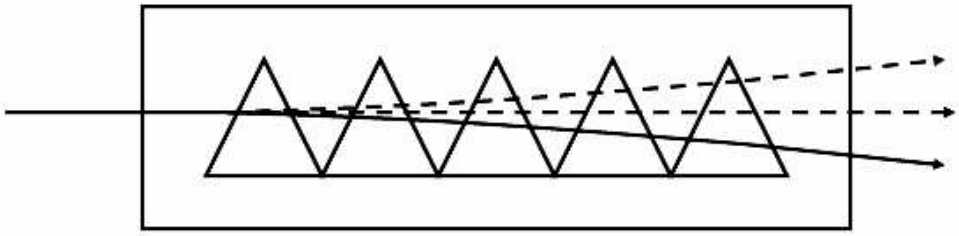

Figure 3.4: Multi-prism beam deflector

Using multiple prisms arranged in series as pictured in Figure 3.4, light deflection angle can be increased. However, the width of the device needs to be increased as more prisms are added. That increase in size becomes a main concern for this rectangular-shaped beam deflector.

Horn-shaped beam deflectors provide the optimum size for maximum deflection. This shape offers a relatively wide deflection angle, while keeping the beam deflector size to be the smallest possible. The size of the beam deflector is just large enough to accommodate the trajectory of the deflected beam [6]. Figure 3.5 shows a horn-shaped ferroelectric beam deflector.

As the deflection angle gets larger, the beam deflector also needs to be wider. The deflection angle contributed by each prism diminishes as the beam deflector gets wider. Multistage deflectors can be utilized instead of one large single-stage deflector. This way, the deflection angle contributed by each prism can be kept relatively high, making efficient use of the drive voltage.

The use of multistage detectors opens the possibility of devices with very large deflection angle. The deflection angle of the beam deflector can be increased

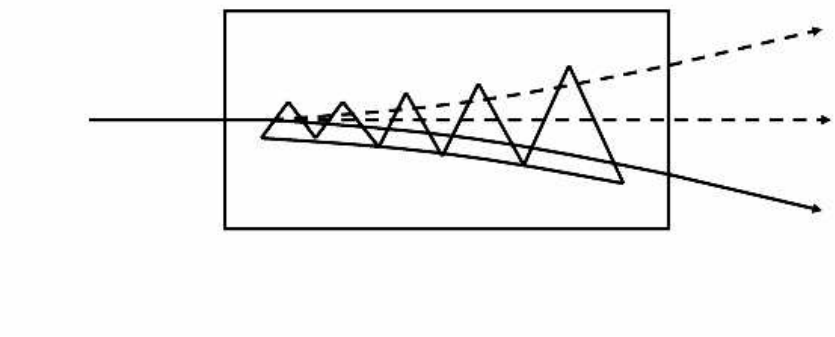

Figure 3.5: Horn-shaped beam deflector

by incorporating additional stages. As another advantage, the drive voltage requirement of the deflector device can be kept relatively low. Multiple channels of lower voltage can be used instead of one channel with extremely high drive voltage. The ferroelectric beam deflector shown in Figure 3.6 is a two-stage device.

3.3 Device Fabrication

The beam deflector device above can be fabricated on a single crystal $LiTaO_3$ wafer that is widely available in the industry. As the first step, a photoresist is patterned on the wafer according to the shape of the deflector. A layer of tantalum metal is then deposited, covering both the photoresist pattern and the exposed crystal. After that, the photoresist is lifted-off to remove the metal layer above it. The remaining metal layer, which covers the area outside of the deflector pattern, is going to be used as an electrode in the domain reversal process.

A layer of photoresist is deposited again in order to reduce the conductivity of the exposed $LiTaO_3$ surface, which helps define the edges of the deflector more accurately [6]. Since the tantalum layer is used as the positive electrode, an electrical contact is made by piercing through this photoresist layer. A uniform water electrode

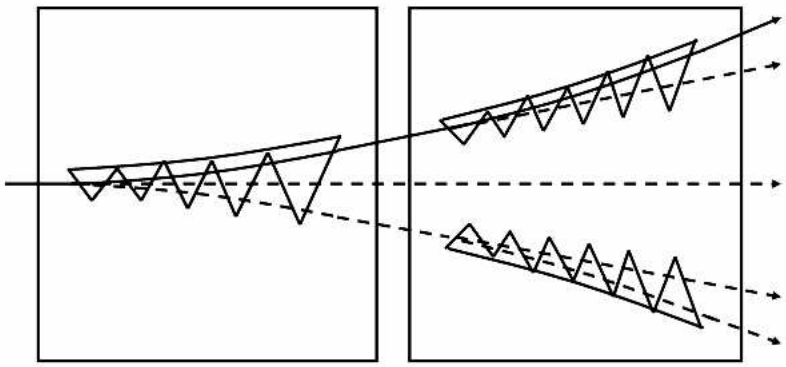

Figure 3.6: A two-stage beam deflector

is used on the other side of the wafer as the negative end. Domain switching is done by applying an electric field with the strength of about 21 kV/mm. After the domain reversal process is finished, the photoresist is removed.

As the last step is the deposition of appropriate electrode pads on both sides of the device. Proper insulating layers are applied to prevent any discharge between electrode pads. Copper tapes are used to provide electrical connection to the electrode pads. The entire device is then encapsulated in silicone.

3.4 Drive Requirements

For the project in this thesis, a two-stage beam deflector device was designed to deflect laser beams with a maximum diameter of 70 μm. In order to accommodate this beam size, the beam deflector was fabricated on a 104$\pm$1μm-thick wafer.

An electric field in the range of $\pm$11 kV/mm will be used to operate the deflector device. This operating field is still below the coercive field of $LiTaO_3$, therefore will not damage the domain pattern of the device. On a 104$\pm$1μm-thick

wafer, an electric field range of ± 11 kV/mm translates to a drive voltage range between 1144 ± 11 V and -1144 ± 11 V.

Since the ferroelectric device only senses the net voltage difference between its electrodes, no voltage reference point is required. The electrodes can be allowed to float freely at any voltage. This is very advantageous, because then the drive voltage requirement can be cut in half. One of the electrodes can be driven to a certain voltage value, while its counterpart on the other side of the device is driven to the same value but in the opposite direction. The net voltage difference sensed by the device will then be twice this value. In other words, the drive voltage does not need to swing the full 2×1144 V in order to provide the required ± 11 kV/mm operating field.

Chapter 4

MULTICHANNEL ±1.16 KV ARBITRARY WAVEFORM GENERATOR DESIGN

As mentioned in Chapter 3, multistage beam deflector devices are designed to produce large deflection angle. In order to operate these devices, however, a special kind of driver is needed.

4.1 Requirements

A multistage beam deflector requires a multichannel high-voltage arbitrary waveform generator with output synchronization capability for its driver. Let us consider the drive voltages needed by a two-stage device in order to steer a laser beam from zero to maximum deflection and back. A two-channel driver is needed for this task. At the start, both output channels are set to zero volts. Then, the first output channel is increased from zero to the maximum voltage while the second is kept at zero. After that, the first channel is held at maximum voltage while the second channel output is increased. For the return to zero deflection, the output voltages are decreased to zero, starting with the second channel first.

All this time, multistage ferroelectric beam deflectors were driven using waveform generators with unsynchronized outputs. These output channels have to be controlled manually. The tedious process of manual control can only be performed for laboratory testing. For practical purposes, the channel synchronization needs to be automated.

The equipment needed to provide those synchronized outputs is not available commercially. A survey of different high-voltage waveform generators has been done. Most of the commercial high-voltage waveform generators have only one output channel. Those with multiple outputs usually do not have enough voltage to drive a ferroelectric beam deflector device, and none of them has the output synchronization capability. Consequently, a custom driver needs to be built.

As mentioned previously in Section 3.4, the deflector device is fabricated on a 104±1μm-thick wafer. In order to drive a device with this thickness, the amplitude of the output channels has to cover a ±1.14 kV range, and each channel has to have the capability to deliver a drive current of 0.4 mA. For the beam deflector application, the resolution of the output voltage has to be quite high, with a maximum step size of 0.31 V. It is also required that the waveform generator be able to work at up to 10 kHz operating frequency.

As an example, Figure 4.1 demonstrates the independent, yet synchronized, waveforms needed to scan the full deflection angle achievable by a two-stage device, like the one shown in Figure 3.6.

4.2 System Design

One of the main reasons for the use of ferroelectric beam deflectors is their small size. Therefore, it is very important to keep the size of the device driver as small as possible. Ideally, the driver would be fabricated as an IC chip and encapsulated in one packaging with the beam deflector device. However, as pointed out earlier, a drive voltage of ±1.14 kV is required. This high voltage requirement renders the chip-level implementation of the driver impossible. Because of that, the implementation of the driver is limited to circuit level, using components that are specifically designed for high-voltage operation.

The driver design in this thesis accomplishes channel synchronization by designating only one component to the task of generating signals for all of the channels.

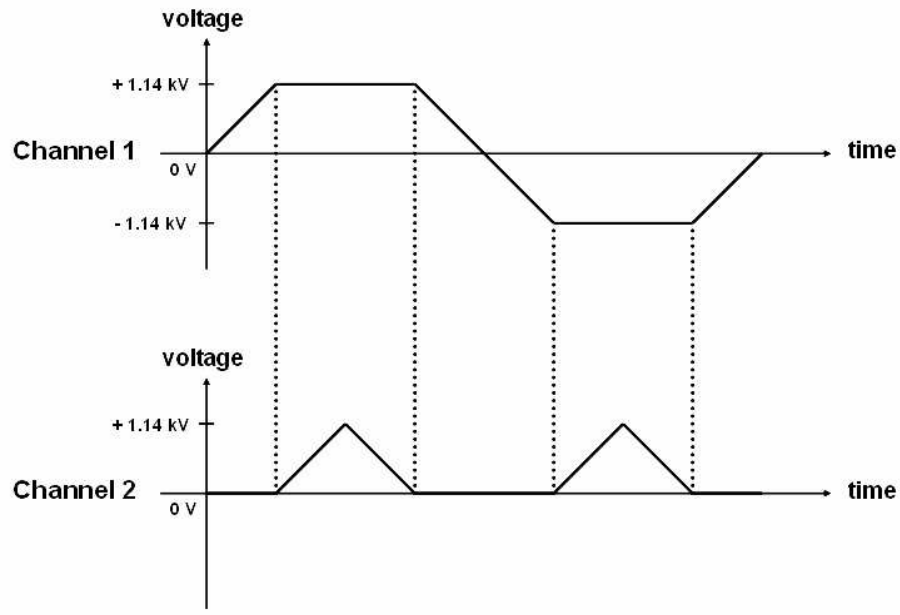

Figure 4.1: Waveforms needed to scan the full deflection angle of the two-stage device in Figure 3.6

These signals are initially generated in digital form. They are then converted to analog using Digital-to-Analog Converters (DACs), and amplified using high-voltage amplifiers.

The driver system comprises two essential sub-systems: an arbitrary waveform generator, and a high-voltage amplifier at each channel. The main component of the arbitrary waveform generator is a Field-Programmable Gate Array (FPGA), while at the core of the high-voltage amplifiers are high-voltage operational amplifiers (op-amps).

4.2.1 Features and Specifications

The utilization of an FPGA in the waveform generator offers programmability. The waveform generator circuit is constructed by programming the configuration of the FPGA. The FPGA configuration can be reprogrammed in the future to change which output channels are used, what kind of waveform generated at each channel, how the outputs relate to one another, etc. More importantly, the reconfiguration process is easy to perform. The FPGA also brings flexibility. With the help of some jumpers and switches, the user can add more functionality into the design, even after the system is completely built.

The high-voltage amplifier design is based on op-amps. This approach brings simplicity and accuracy to an amplifier design. The use of high-voltage op-amps instead of discrete transistors helps in reducing the component count. With fewer components, the driver size is minimized. The design complexity is also reduced, making it more reliable, and provides better control on the accuracy of the amplifier. The design also features fine-tuning of the amplifier gain at each channel by using trimpots.

All of the components used in the design are commercially available parts. They are put together on a single board, and protected in a metal enclosure. The design data are available at: http://www.cvorg.ece.udel.edu/stabboard

These data can be used by ferroelectric device researchers to build high-voltage drivers that meet their specific device and application requirements (e.g., number of output channels, maximum voltage, resolution, and operating speed).

With appropriate component selection, the driver is designed to meet or exceed the requirements of the beam deflector device and application. This waveform generator has five output channel, each capable of producing an arbitrary ±1.16 kV signal that is resolvable in 65,536 steps. Each channel has a 10 mA drive capability. The operating frequency of this driver can be varied from 0 to 10 kHz.

4.2.2 Architecture

The architecture of the driver is shown in Figure 4.2. An FPGA handles the arbitrary waveform signal generation. By using a single, appropriately sized FPGA, synchronization of multiple waveforms is simplified while minimizing cost. An Electrically Programmable Read-Only Memory (EPROM) is used to store the configuration of this FPGA. User inputs are needed to choose the type and frequency of the waveform generated. In order to provide feedback to the user, the status of operation of the waveform generator is displayed using alphanumeric Light Emitting Diode (LED) displays. The digital signal outputs from the FPGA are converted to analog signals using DACs. High-voltage signals are finally obtained by amplifying the outputs of the DACs.

4.3 Design Subsystems

The job of the driver system can be divided into three main tasks: waveform generation, signal amplification, and user interface. In order to make it easier to understand, the driver system is divided into three subsystems according to these tasks.

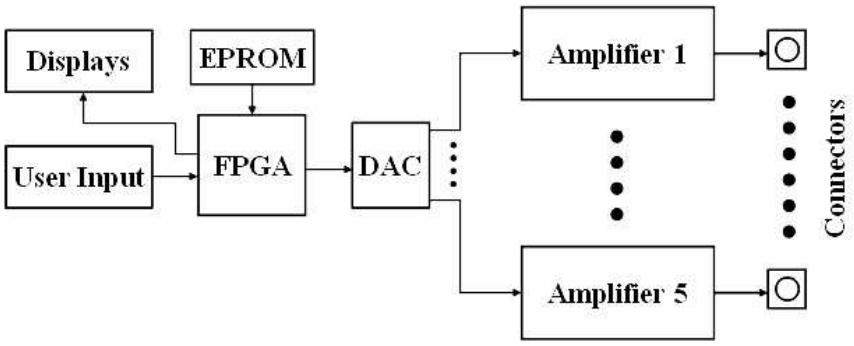

Figure 4.2: Architecture for the multichannel ±1.16 kV arbitrary waveform signal generator

4.3.1 FPGA-Based Arbitrary Waveform Generator

An FPGA is used to generate 16-bit digital signals, which will then be converted to analog signals using 16-bit DACs. An FPGA can be considered as a configurable digital circuit. It contains a large number of digital logic gates and memories. A lot of the connections between these components are programmed using a configuration file.

There are a number of ways to get this configuration file. Most commonly, the functionality of the FPGA is first written in a Hardware Description Language (HDL). The description is then synthesized into the configuration file using a synthesis software. Next, the resulting file is downloaded into an EPROM—for non-volatile storage—using an EPROM programming software. Everytime the system is started up, the FPGA accesses the configuration file inside this EPROM.

The FPGA can be reconfigured quite easily. The user only needs to synthesize a new HDL code which is going to be downloaded into the configuration EPROM. The FPGA will automatically access this new configuration file at the next start.

Figure 4.3 illustrates the structure of the HDL code used for the work in

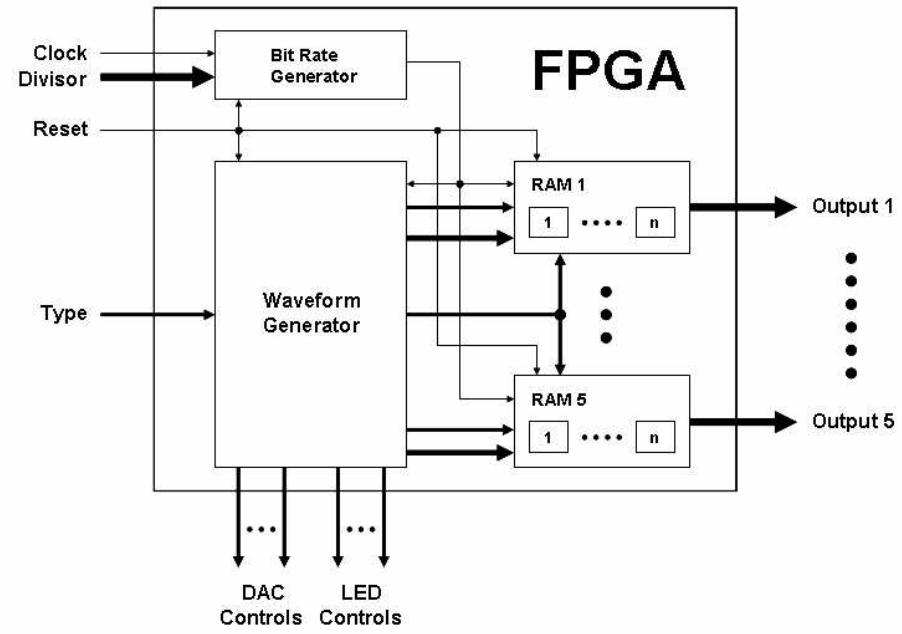

Figure 4.3: HDL code structure for the configuration of the FPGA

this thesis. Sampled arbitrary waveforms are stored in the Random Access Memories (RAMs) inside the FPGA. There are five blocks of RAM—one for each output. There can be more than one waveforms stored for each channel. An input from the user chooses the waveform type.

The FPGA generates the waveforms by reading the stored sample points and sending the required control signals for DAC to read them. It repeats the process after all the sample points are read, to generate a periodic waveform. The FPGA also controls the alphanumeric displays to show the operating status of the waveform generator. The user may select the output frequency by controlling how fast the waveform generator reads the sample point values. This is achieved by scaling the clock frequency inside the FPGA.

The HDL code is first analyzed and simulated for functionality using VHDL[1] System Simulator (VSS) software from Synopsys, Inc. After successful simulation, the code is then *synthesized* (translated into logic gates and optimized for the target device) using Foundation Series software, a set of design tools from Xilinx, Inc. The resulting file is then formatted for the right EPROM and downloaded from a Personal Computer (PC) into the EPROM using PROM File Formatter software and Joint Test Action Group (JTAG) Programmer download cable, both also available from Xilinx, Inc.

The HDL code and the synthesized result are available at:
http://www.cvorg.ece.udel.edu/stabboard/vhdl
It should be noted that the HDL code above is only a sample. The user can always use other algorithms for generating the signals.

The FPGA used in the waveform generator is an XCV600E device from Xilinx, Inc. It has 985,882 logic gates, a 48×72 array of Configurable Logic Blocks (CLBs), 294,912 bits of block RAM, and 221,184 bits of distributed RAM, which are sufficient for the implementation of the waveform generator [23]. This device comes in Ball Grid Array (BGA) package with 316 user Input/Output (I/O) lines, providing flexibility for the design.

An XC18V04 EPROM device from Xilinx, Inc. is used to store the configuration file for the FPGA. It has a capacity of 4,194,304 bits, large enough for the configuration file of XCV600E, which is 3,961,632 bits [24]. XC18V04 is an in-system-programmable configuration EPROM. Programming this EPROM does not require its removal from the system. This feature is very important to facilitate the process of reconfiguration of the FPGA.

The schematic of the FPGA programming circuit is shown in Figure 4.4.

[1] This is a case of an acronym inside an acronym. VHDL stands for VHSIC Hardware Description Language, where VHSIC stands for Very High Speed Integrated Circuit.

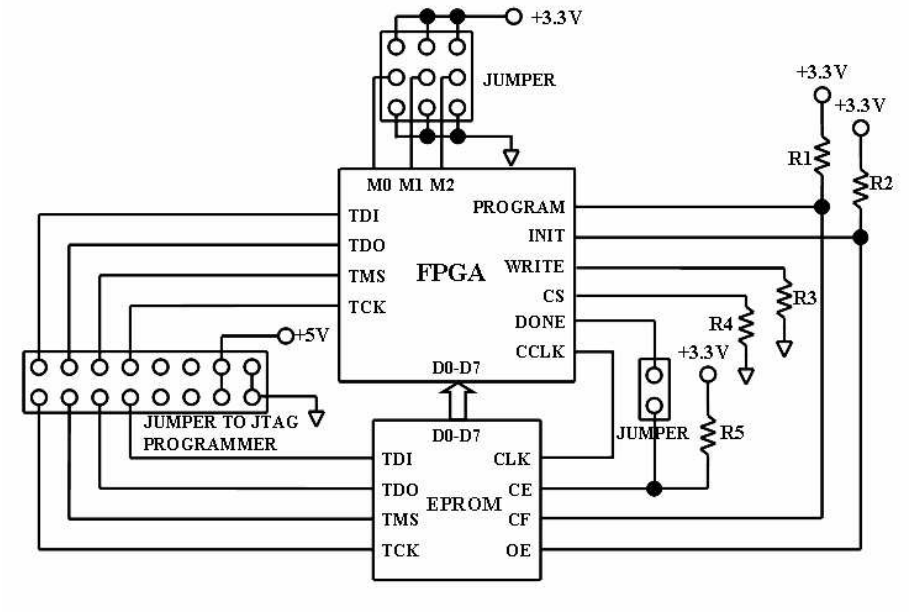

Figure 4.4: Schematic of the FPGA programming circuit

When programming the EPROM, the circuit is connected to the JTAG Programmer, the DONE pin of the FPGA is disconnected from the CE pin of the EPROM, and the M2, M1, and M0 pins can be left open. For driver operation after the EPROM is programmed, the JTAG Programmer is removed, the DONE pin of the FPGA is connected to the to the CE pin of the EPROM, the M2 pin of the FPGA is connected to +3.3 V, whereas the M1 and M0 pins are connected to ground. The value of the components used for this FPGA programming circuit can be seen in Table 4.1.

The DACs used in the design are AD7846 devices from Analog Devices, Inc. These devices feature high resolution output of 16-bit, monotonicity over temperature, and high accuracy required by the beam steering application [25]. The design uses an AD588 device—also from Analog Devices, Inc.—to provide a high-precision voltage reference.

Table 4.1: Part list for the FPGA programming circuit

Parts	**Label**	**Value/Type**
Pull-up resistor	R_1	4.7 kΩ
Pull-up resistor	R_2	4.7 kΩ
Pull-down resistor	R_3	1 kΩ
Pull-down resistor	R_4	1 kΩ
Pull-up resistor	R_5	300 Ω
Field-Programmable Gate Array	FPGA	XCV600E
Configuration EPROM	EPROM	XC18V04

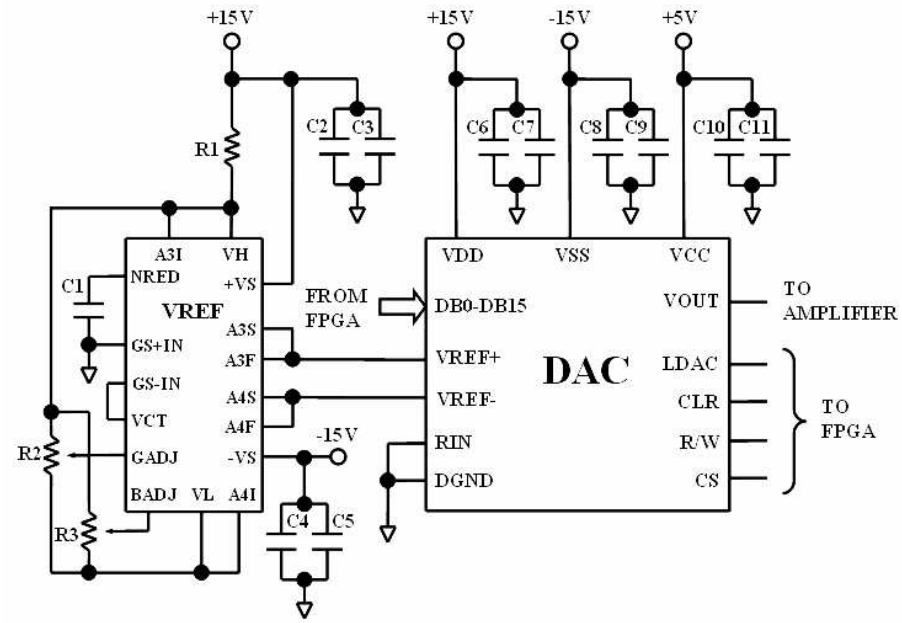

Figure 4.5: Schematic for the DAC circuit

Table 4.2: Part list for the DAC circuit

Parts	**Label**	**Value/Type**
Pull-up resistor	R_1	39 kΩ
Gain adjustment trimpot	R_2	10 kΩ
Balance adjustment trimpot	R_3	100 kΩ
Noise reduction capacitor	C_1	1 μF
Bypass capacitors	C_2, C_4, C_6, C_8, C_{10}	10 μF
Bypass capacitors	C_3, C_5, C_7, C_9, C_{11}	0.1 μF
Digital-to-Analog Converter	DAC	AD7846
Voltage reference IC	VREF	AD588

The schematic for the DAC circuit is shown in Figure 4.5. The parts used for this circuit are listed in Table 4.2. Generally, the AD588 will meet the requirements of a precision system without additional adjustment. Initial output error of 1 mV and output noise specifications of 10 μV peak-to-peak allows for accuracies of 12–16 bits [26]. However, for an even greater level of accuracy, additional calibration can be performed using the gain adjustment and balance adjustment trimpots (R_2 and R_3, respectively).

4.3.2 High Voltage Amplifier

The DAC outputs are ±10 V analog signals. These signals needs to be amplified to ±1.14 kV using high-voltage amplifiers. In the waveform generator design, five high-voltage amplifiers are used—one for each channel.

These high-voltage amplifiers are constructed by using two op-amps connected in a bridge configuration, as depicted in Figure 4.6. The op-amps used in the high-voltage amplifiers are the PA89 devices from Apex Microtechnology Corp.

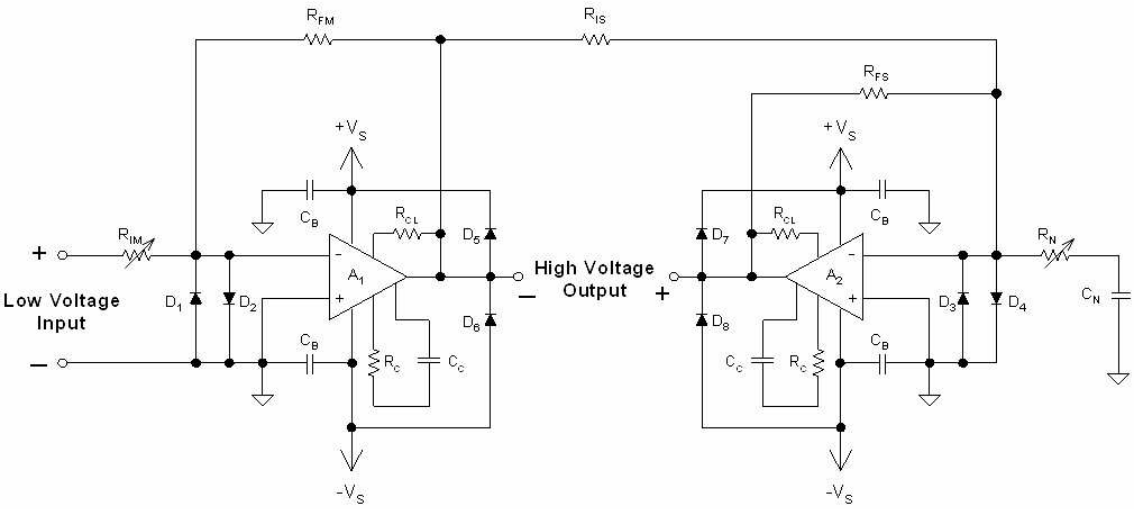

Figure 4.6: Schematic of the high-voltage amplifier section

These op-amps use hybrid technology[2] in order to be able to produce ±580 V output signals [27]. By using the bridge configuration, ±1.16 kV output signals can be obtained [3].

In a bridge configuration, when one op-amp output swings to a value, the other swings to the same value, only with the opposite polarity. The output of the amplifier is the difference between the outputs of the two op-amps. Therefore, the total output is twice the magnitude of each op-amp output. A benefit that can be taken from this mechanism is that the required supply voltage range is only one half of the maximum output swing.

The gain of the amplifier can be tuned by adjusting the input varistor R_{IM}. The value of R_{FM}/R_{IM} is half of the multiplication factor for the output voltage. The op-amps allow a maximum multiplication factor of 116. For the project in this thesis,

[2] A hybrid op-amp is enclosed in a small packaging comparable to that of monolithic op-amp, but the high-power components and the low-power components inside the packaging are fabricated on separate substrates.

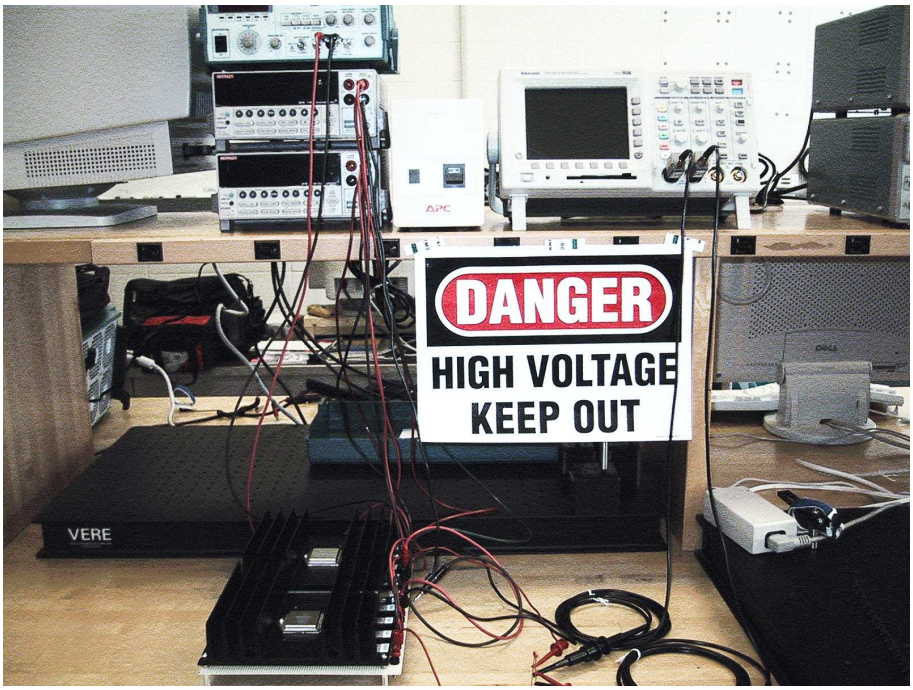

Figure 4.7: High-voltage amplifier test setup

the value of the varistor R_{IM} and resistor R_{FM} are set so that the multiplication factor is 114. This way, a ±10 V input produces a ±1.14 kV output. Varistor R_N and capacitor C_N are used for noise gain compensation. The value of R_N has to be equal to the value of R_{IM}.

A test circuit has been built to examine the performance of this amplifier before it is used in the waveform generator. Figure 4.7 shows the high-voltage amplifier test setup. A sample output waveform for a ±10 V triangular input with R_{FM}/R_{IM} set at 50 can be seen in Figure 4.8. Table 4.3 lists the components used for the high-voltage amplifier.

Heatsinks and thermal washers are used to help with heat dissipation. In order to prevent short circuits to the heatsinks and washers, the pins of the op-amps are sleeved with Teflon tubing. The heatsinks are model 396-2AB from Wakefield

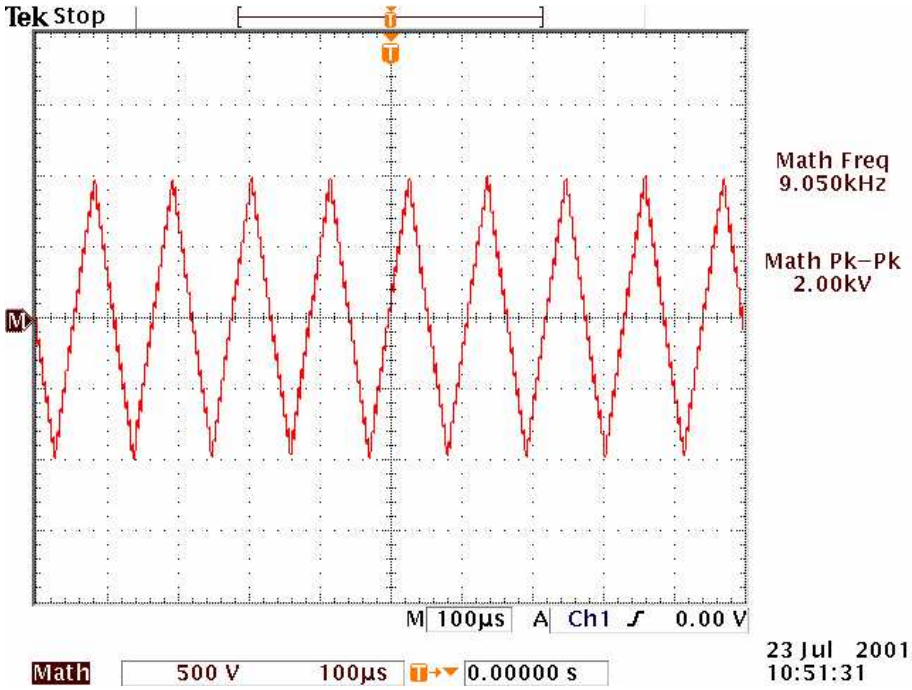

Figure 4.8: High-voltage amplifier output waveform

Table 4.3: Part list for the high-voltage amplifier

Parts	**Label**	**Value/Type**
Input varistor	R_{IM}	1-20 kΩ
Input protection diodes	D_1, D_2, D_3, D_4	1N4148
Main feedback resistor	R_{FM}	500 kΩ
Bypass capacitors	C_B	0.1 μF (600 V)
Op-amps	A_1, A_2	PA89
Current limit resistor	R_{CL}	23.2 Ω
Compensation capacitor	C_C	33 pF (3 kV)
Compensation varistor	R_C	220 Ω
Output protection diodes	D_5, D_6, D_7, D_8	RHRP15120
Secondary interface resistor	R_{IS}	500 kΩ
Secondary feedback resistor	R_{FS}	500 kΩ
Noise gain compensation varistor	R_N	1-20 kΩ
Noise gain compensation capacitor	C_N	560 pF

Thermal Solutions, Inc, and the thermal washers are model TW05 from Apex Microtechnology Corp. The tubing is type TSI-S22-1100-NAT from SPC Technology. It has a wall thickness of 12±2 mil with dielectric strength of more than 1,400 V/mil, far above the requirement of the design.

4.3.3 Support Components

In addition to the FPGA-based waveform generator and the high-voltage amplifier, some support components are added. Push button and Dual In-line Package (DIP) switches, hexadecimal LED displays, and headers—for jumpers—are added for design flexibility. The user can customize their usage by modifying the HDL code. In this driver design, some of them are used as waveform and frequency selectors. One of the push buttons is used as a reset button.

There are six LED displays in the design. They are used to display the status of operation of the driver. One of them displays the operating status of the FPGA. The other five display the status of each output channel.

The displays used are HDSP-0762 from Agilent Technologies, Inc. These displays have internal code converters inside them. Because of this, they use binary code for the data inputs, simplifying the HDL code writing. A blanking control is used to turn the LED display off for each unused channel.

4.4 System Integration

The multichannel driver system is integrated on a seven-layer Printed Circuit Board (PCB). The PCB is designed using PCBoards PCB design software, part of DesignLab integrated design tools from MicroSim Corp. For replaceability and reusability, the critical components (i.e., FPGA, EPROM, DACs, voltage reference IC, clock crystal, high-voltage op-amps, and LED displays) are mounted on sockets.

The waveform generator is fitted inside a metal enclosure for protection and portability. Two fans are installed in the enclosure for air circulation to dissipate

Figure 4.9: Five-channel high-voltage amplifier

the heat from the system. Using screws and spacers, the heatsinks are attached to the board, which is then attached to the enclosure. Coaxial Miniature High-Voltage (MHV) connectors are used for the high-voltage outputs. These connectors are rated to 5 kV. For power supplies, banana jacks are used. A photograph of the completed ±1.16 kV waveform generator is shown in Figure 4.9.

4.5 System Testing

Partial functionality tests were carried out as the driver was being built. The board assembly was started from the FPGA-based waveform generator subsystem and the alphanumeric displays. After the completion of this subsystem, some tests were performed. With the help of alphanumeric displays, the functionality of the FPGA programming mechanism can be assured. The outputs of the DACs were

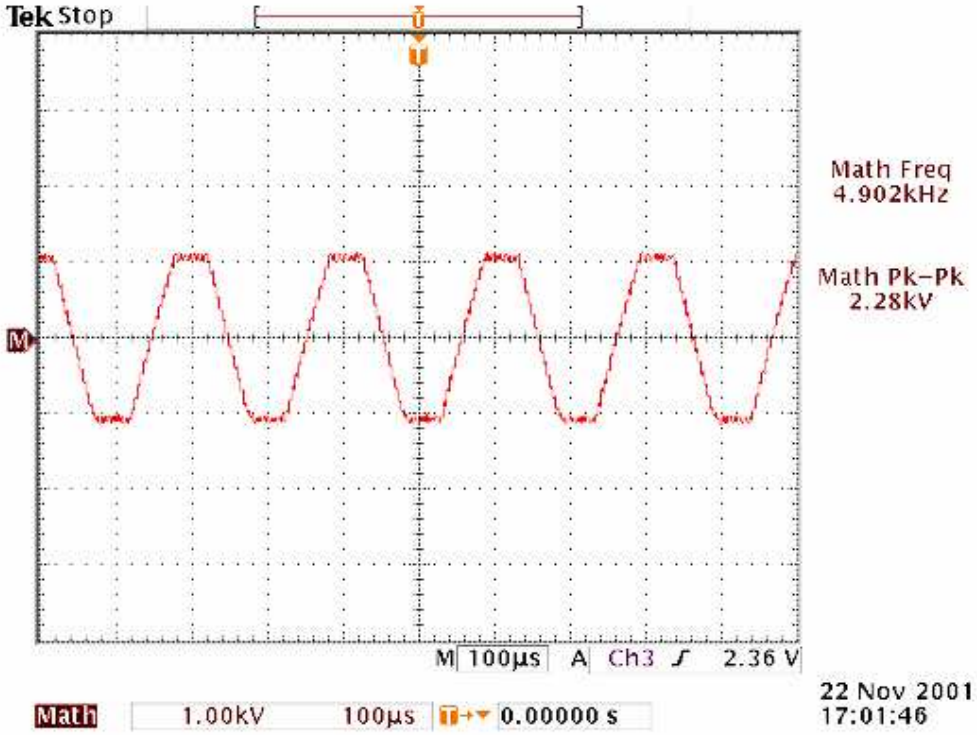

Figure 4.10: High-voltage driver output waveform for Channel 1

tested for proper waveform shaping. After the system was completely built, a number of tests were done to produce different waveforms on each channel at different voltages and frequencies, starting from low to high.

The design have been tested to drive a two-stage $LiTaO_3$ ferroelectric beam deflector. Figure 4.10 and 4.11 show the waveforms used to scan the full deflection angle of a two-stage ferroelectric device at 5 kHz. Each channel of the waveform generator output is capable of producing ± 1.16 kV at 10 kHz; therefore, the scanning frequency for two stages together is 5 kHz.

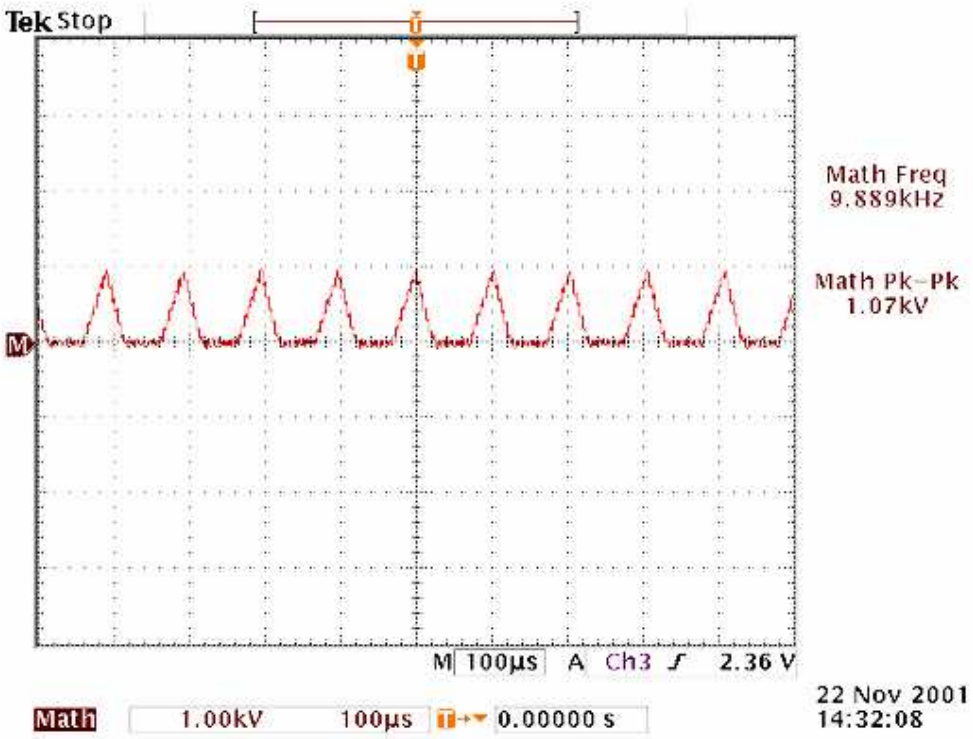

Figure 4.11: High-voltage driver output waveform for Channel 2

The waveforms above were captured using TDS3014 oscilloscope from Tektronix, Inc. With special high-voltage probes to scale the input down to $\frac{1}{10}$ of the original value, the oscilloscope can measure up to 1.5 kV voltage range with 9-bit vertical accuracy [28]. The output of the waveform generator was measured by using two high-voltage probes—one for positive end, one for negative end. A mathematical function in the oscilloscope was utilized to calculate the difference between the voltages measured by these probes.

Figure 4.12: Laser beam deflection test

In Figure 4.12 can be seen the setup for laser beam deflection test using multistage ferroelectric device. In this experiment a total deflection angle of 25.4° (±12.7°) was demonstrated. Deflection angle this large is unprecedented for electro-optic scanning [1]. With five independent high-voltage outputs, a total deflection angle of 60°—about 12.5° per stage—could be achieved when driving a five-stage ferroelectric beam deflector.

Chapter 5

FUTURE DIRECTION

Using the waveform generator design, the use of current generation multistage ferroelectric beam deflectors has been successfully demonstrated. This driver was developed because there was no suitable commercial equipment available. The lack of driver with synchronizable output is a challenge for all researchers who develop multistage ferroelectric beam steering devices. As previously discussed, the design can be readily adapted by these researchers to build high-voltage drivers that meet their specific device and application requirements.

The research on heterogeneously integrated beam steering device is still in its early development stage. In the future, there are some improvements that can be done, both on the device and the driver.

5.1 Next Generation Device

The most important works that can be done on the beam deflector device are increasing the maximum deflection angle and lowering the maximum required drive voltage.

5.1.1 Additional Deflector Stages

The most straightforward method to increase the maximum deflection angle is by incorporating additional stages. The driver design described in this thesis can support up to five stages. By using five stages, the maximum deflection angle of around 62.5° can be obtained.

As an even further development, another type of deflector array can be considered. One of them is the pizza type deflector. In this arrangement, several deflectors are placed side by side forming a circle, resembling the slices of a pizza or the spokes in a wheel. Fiber optic selection module is used to determine which deflector is used. This way, a full 360° deflection in the horizontal plane can be achieved. This deflector can then be combined with MEMS-controlled micro-mirrors placed at the end of each ferroelectric beam deflector, either at the hub or at the rim. These micro-mirrors can be used to cover the deflection in the vertical plane. This combination covers a hemispherical field of regard, which can deflect laser beams to anywhere over the horizon.

5.1.2 Lower Drive Voltage

Active research is underway to reduce the drive voltage requirements for ferroelectric devices. One of the options that can be considered is by using a thinner wafer. Using a 10-μm-thick crystal, the required drive voltage can be brought down to around 160 V. The wafer can be cut this thin by crystal ion slicing method. On this thin wafer, the required current per channel will be 4 mA, which can be provided by the current driver design.

The drive voltage requirements can also be reduced by using alternative materials such as strontium barium niobate (SBN). SBN has a higher electro-optic coefficient, which leads to higher deflection angle. With higher deflection angle per stage, the required number of stages can be reduced, or the voltage requirement can be reduced for the same angle.

When the drive voltages are reduced below 100 volts, an Integrated Circuit (IC) implementation becomes possible. With this approach, the entire driver is built on a single chip using commercially available high-voltage IC fabrication process, such as the one offered by austriamicrosystems AG [30]. This integrated approach have also been taken for use with lower voltage beam steering devices

(SLM and MEMS) [4]. The high-voltage CMOS process offered by austriamicrosystems is available to the public through their Multi Product Wafer (MPW) program. In this program, multiple customers submit their design to be fabricated on the same silicon wafer.

However, the complexity and the cost associated with low-volume IC production in order to take this approach may not be warranted by researches primarily focused on ferroelectric device development. Additionally, as new ferroelectric devices are developed, the scalability and customizability of the discrete design approach makes it an attractive substitute to commercial equipments operating at low voltages.

5.2 Driver Integration

For the device driver, the main concern is to get the size as small as possible. The size of the driver can be reduced to the smallest possible size by implementing the beam deflector on an IC chip. As previously mentioned, austriamicrosystems offered a solution for drive voltages below 100 volts. For higher voltages, some other high-voltage silicon wafer manufacturing processes might be considered as alternatives.

A survey on the industry indicates that some companies have developed high-voltage device technologies that are promising to be used for driver integration. Apex Microtechnology Corp. provides a method of hybrid packaging of high voltage devices. There is BCDSOI process by STMicroelectronics, Inc. A silicon process called EZ-HV is developed by Philips Semiconductors N.V. Another alternative is using silicon carbide (SiC) or galium nitride (GaN) technology. These manufacturing processes are not commercially available, but they open the possibility of fully integrated driver design.

The hybrid packaging offered by Apex Microtechnology provides the possibility to integrate low-voltage and high-voltage devices in a small package. It is not

a total integration where the devices are fabricated on the same die. Instead, those devices are fabricated on separate dice. They are then connected to one another using wire bonding, and enclosed in one packaging. Using this technology, the logic circuits can be inserted into the high voltage op-amp package. Although this approach does not provide the smallest size, it is the most straightforward and gives the highest output voltage.

STMicroelectronics develops their "smart power" devices by integrating Bipolar, CMOS, and DMOS (BCD) transistor circuits on a single chip. Their BCD6 process integrates 40 V/20 V power DMOS transistors with 0.35 μm, CMOS-based Microcontroller Units (MCUs), logic circuits, and nonvolatile memory, also with bipolar transistors for control/protection functions. By implementing their BCD process on the Silicon on Insulator (SOI) technology, 200 V/700 V circuits can be expected.

The EZ-HV process from Philips Semiconductor is capable of merging 650 V DC power devices (or 270 V AC) with standard low-voltage logic and linear devices on the same SOI chip. This outstanding feature is attained by using a counter-intuitive thinking. Traditionally, high-voltage devices are created by using a thick layer of silicon to delay the onset of the critical-field conditions that cause impact ionization leading to avalanche breakdown. Philips takes an entirely different approach. Their EZ-HV process uses a thin layer instead. In a thin layer, there are fewer atoms. With fewer atoms, the supply of electrons and holes caused by impact ionization is limited. This in turn prevents avalanche breakdown.

Researches on SiC and GaN materials are conducted to exploit their high breakdown voltage. It has been shown that SiC devices can be shrunk to submicron dimensions. Consequently, CMOS circuits and high-power devices can be built on the same substrate.

All of the process technologies above have some limitations. Integrating the

driver using those technologies may not be as easy as desired. However, those processes give us some encouraging prospect that in the future, driver integration is indeed possible.

REFERENCES

[1] D. Scrymgeour, A. Sharan, V. Gopalan, K. Gahagan, R. Sander, J. Robinson, F. Muhammad, P. Chandramani, and F. Kiamilev. Cascaded electro-optic scanning of laser light over large angles using domain microengineered ferroelectrics. *Applied Physics Letters*, 81(17):3140–3142, October 2002.

[2] F. Muhammad, P. Chandramani, J. Ekman, F. Kiamilev, D. Scrymgeour, V. Gopalan, E. Moore, and M. Weiler. Multi-channel ±1.1kV arbitrary waveform generator for beam steering using ferroelectric device. *IEEE Photonics Technology Letters*, 14(11):1605–1607, November 2002.

[3] F. Muhammad, P. Chandramani, J. Ekman, F. Kiamilev, V. Gopalan, E. Moore, and M. Weiler. Compact multichannel 2kV arbitrary waveform generator for ferroelectric device arrays. In *2001 IEEE/LEOS Annual Meeting Conference Proceedings*, volume 2, pages 818–819, November 2001.

[4] P. Chandramani, F. Muhammad, J. Ekman, F. Kiamilev, E. Moore, and M. Weiler. High-voltage CMOS arbitrary waveform generator for linear SLM array. In *2001 IEEE/LEOS Annual Meeting Conference Proceedings*, volume 2, pages 451–452, November 2001.

[5] M. Weiler, J. Ahearn, S. Adams, T. McElwain, A. Stark, L. DePaulis, A. Sarafinas, T. Hongsmatip, R. Martin, and B. Lane. Large scale modulator arrays for beam steering and optical modulator applications. In *2001 IEEE/LEOS Annual Meeting Conference Proceedings*, volume 2, pages 808–809, November 2001.

[6] D. Scrymgeour, Y. Barad, V. Gopalan, K. Gahagan, Q. Jia, T. Mitchell, and J. Robinson. Large angle electro-optic laser scanner on $LiTaO_3$ fabricated by in-situ monitoring of ferroelectric domain microengineering. *Applied Optics*, 40(34):6236–6241, December 2001.

[7] J. Valasek. *Physical Review*, 15:537, 1920.

[8] J. Valasek. *Physical Review*, 17:475, 1921.

[9] C. Sawyer and C. Tower. *Physical Review*, 35:269, 1930.

[10] J. Sinha. *Journal of Scientific Instruments*, 42:696, 1965.

[11] J. Anderson. *Dielectrics*. Modern Electrical Studies. Chapman and Hall Ltd., London, 1964.

[12] A. von Hippel, editor. *Dielectric Materials and Applications*. The Technology Press of M.I.T. and John Wiley & Sons, Inc., New York, 1954.

[13] P. Harrop. *Dielectrics*. Butterworth & Co. Ltd., London, 1972.

[14] A. von Hippel. *Dielectrics and Waves*. John Wiley & Sons, Inc., New York, 1954.

[15] M. Howard and D. Howard. Introduction to crystallography and mineral crystal systems. [Online], 1998.
Available at http://www.rockhounds.com/rockshop/xtal.

[16] M. Lines and A. Glass. *Principles and Applications of Ferroelectrics and Related Materials*. The International Series of Monographs on Physics. Oxford University Press, Oxford, 1977.

[17] Y. Xu. *Ferroelectric Materials and Their Applications*. North-Holland, Amsterdam, 1991.

[18] R. Elliott. *Electromagnetics: History, Theory, and Applications*. IEEE/OUP Series on Electromagnetic Wave Theory. IEEE Press and Oxford University Press, New York, 1993.

[19] E. Fatuzzo and W. Merz. *Ferroelectricity*, volume VII of *Series of Monograph on Selected Topics in Solid State Physics*. John Wiley & Sons, Inc., New York, 1967.

[20] R. Johnstone. Matsushita's gamble. *Technology Review*, 107(3):26, April 2004.

[21] V. Gopalan and M. Gupta. Observation of internal field in $LiTaO_3$ single crystals: Its origin and time-temperature dependence. *Applied Physics Letters*, 68(7):888–890, February 1996.

[22] C. Davis. *Laser and Electro-optics: Fundamentals and Engineering*. Cambridge University Press, New York, 1996.

[23] Xilinx, Inc. *Virtex^{TM}-E 1.8 V Field Programmable Gate Arrays v2.0*, April 2001.
Available at http://www.xilinx.com.

[24] Xilinx, Inc. *XC18V00 Series of In-System Programmable Configuration PROMs v2.8*, June 2001.
Available at http://www.xilinx.com.

[25] Analog Devices, Inc. *LC ^{2}MOS 16-Bit Voltage Output DAC AD7846 Rev.E*, 2000.
Available at http://www.analog.com.

[26] Analog Devices, Inc. *High Precision Voltage Reference AD588 Rev.B*, 1986.
Available at http://www.analog.com.

[27] Apex Microtechnology Corp. *Power Integrated Circuits Data Book vol.9*, 2000.
Available at http://www.apexmicrotech.com.

[28] Tektronix, Inc. *Digital Phosphor Oscilloscopes: TDS3012, TDS3014, TDS3032, TDS3034, TDS3052, TDS3054*, April 2000.
Available at http://www.tektronix.com.

[29] L. Sun, J. Kim, C. Jang, D. An, X. Lu, Q. Zhou, J. Taboada, R. Chen, J. Maki, S. Tang, H. Zhang, W. Steier, C. Zhang, and L. Dalton. Polymeric waveguide prism-based electro-optic beam deflector. *Optical Engineering*, 40(7):1217–1222, July 2001.

[30] austriamicrosystems AG. High-voltage processes CXJ–CXO. [Online].
Available at http://www.austriamicrosystems.com.

[31] A. Bindra. Intelligent power ICs tout system-level integration. *Electronic Design*, 47(26), December 1999.